Error-Free Matthiessen's Rule in the MOSFET Universal Mobility Region

Ming-Jer Chen, *Senior Member, IEEE*, Wei-Han Lee, *Student Member, IEEE*, and Yi-Hui Huang

***Abstract*—Through the experimentally validated inversion-layer mobility simulation, we devise an error-free version of Matthiessen's rule for a single-gate n-channel bulk MOSFET in the universal mobility region. The core of the new rule lies in a semi-empirical model, which explicitly expresses the errors due to the conventional use of Matthiessen's rule as a function of both the lowest subband population and the relative strength of individual mobility components. The model holds under practical conditions (with temperatures up to 400 K) and in a broad range of substrate doping concentrations (10^{14} to 10^{18} cm^{-3}). To make the error-free proposal more general, we elaborate on several issues, including strain, impurity Coulomb scattering, and remote scattering. The thin-film case can be treated accordingly.**

***Index Terms*—Matthiessen's rule, metal–oxide–semiconductor field-effect transistors (MOSFETs), mobility, model, scattering, simulation, strain, universal mobility.**

I. Introduction

TO PROBE individual scattering mechanisms in the inversion layers of MOSFETs, Matthiessen's rule may be favored because of its additive property of reciprocal mobility components. As pointed out earlier by Stern [1], however, there will be errors of more than 15% due to the use of Matthiessen's rule for temperatures over 40 K. Since then, there have been four fundamentally different methods published in the literature concerning the validity and applicability of Matthiessen's rule [2]–[7]. First, Matthiessen's rule must be carried out under extreme or impractical conditions such as very low temperatures (near absolute zero) [2]. Second, sophisticated numerical simulations on individual mobility components were instead used, with no need to account for Matthiessen's rule [3]. Third, for the engineering purpose, the errors caused by Matthiessen's rule were overlooked while assessing mobility components individually [4], [5]. Fourth, mobility simulations were performed to deliver the errors of the mobility components extracted using the rule, with [6] and without [3], [7] the inclusion of ionized impurity Coulomb scattering.

It is noteworthy that Stern [1] had suggested the relative strength of individual mobility components as one origin of the errors. The other origin in terms of the subband population had also been put forward by Fischetti *et al.* [3]. The combination of these two origins should enable the creation of a fifth method in the field.

Herein, we propose such a new method in terms of an error-free version of Matthiessen's rule. The establishment of the method is demonstrated in a single-gate bulk structure in the universal mobility region, with the practical situations (different temperatures and different doping concentrations) taken into account. To make possible the general applications of the error-free proposal, we elaborate on such issues as strain, impurity Coulomb scattering, and remote scattering. The thin-film case is also addressed.

II. Simulation Framework and Error Definition

We previously established a sophisticated simulation package [7]–[10] in the context of a silicon conduction-band structure with six constant-energy surfaces [11]. This package was dedicated to a single-gate bulk structure, consisting of a self-consistent Poisson and Schrödinger's equations solver in the confinement direction [8] and an inversion-layer mobility calculation program [7], [9], [10]. The outcomes of the former include the subband level, the Fermi level, and the wave function, all of which serve as inputs to the latter to calculate the electron inversion-layer mobility.

In the mobility calculation, the momentum relaxation time approximation [12], [13] was made. Thus, for the thick gate oxide case where three well-known scattering mechanisms prevail, the total energy-dependent relaxation time $\tau_{\rm tot}$ can be expressed as a function of the relaxation time $\tau_{\rm ph}$ due to phonon scattering alone, the relaxation time $\tau_{\rm sr}$ due to surface roughness scattering alone, and the relaxation time $\tau_{\rm imp}$ due to impurity Coulomb scattering alone, i.e.,

$$\frac{1}{\tau_{\rm tot}^{ij}(E)} = \frac{1}{\tau_{\rm ph}^{ij}(E)} + \frac{1}{\tau_{\rm sr}^{ij}(E)} + \frac{1}{\tau_{\rm imp}^{ij}(E)} \tag{1}$$

where $j = 1$ represents the twofold valley $\Delta 2$, $j = 2$ represents the fourfold valley $\Delta 4$, and i represents the corresponding subband number. The literature formalisms for $\tau_{\rm ph}$ [14], $\tau_{\rm sr}$ [15], and $\tau_{\rm imp}$ [16], [17] were quoted. The corresponding mobility of subband i of valley j can be calculated [12] as

$$\mu_x^{ij} = \frac{q\int_{E_{ij}}^{\infty}(E-E_{ij})\tau_x^{ij}(E)\left(\frac{\partial f}{\partial E}\right)dE}{m_{\rm cj}\int_{E_{ij}}^{\infty}(E-E_{ij})\left(\frac{\partial f}{\partial E}\right)dE} \tag{2}$$

where x stands for ph, sr, or tot in (1), E_{ij} represents the energy level of subband i of valley j, $m_{\rm cj}$ represents the

Manuscript received August 23, 2012; revised November 8, 2012; accepted December 4, 2012. Date of publication January 1, 2013; date of current version January 18, 2013. This work was supported by the National Science Council of Taiwan under Contract NSC 101-2221-E-009-057-MY3. The review of this paper was arranged by Editor H. Shang.

The authors are with the Department of Electronics Engineering and Institute of Electronics, National Chiao Tung University, Hsinchu 300, Taiwan (e-mail: chenmj@faculty.nctu.edu.tw).

Color versions of one or more of the figures in this paper are available online at http://ieeexplore.ieee.org.

Digital Object Identifier 10.1109/TED.2012.2233202

conductivity effective mass [11] of valley j, and f represents the Fermi–Dirac distribution. Note that the parabolic band approximation, the isotropic scattering approximation, the elastic scattering approximation (for $\tau_{\rm sr}$ and $\tau_{\rm imp}$), and the momentum relaxation time approximation have all be used in this paper dedicated primarily to the single-gate bulk structure. Extension to the thin-film structure is possible, as will be explained later.

By going through all subbands and valleys, the total mobility and the individual mobility components can be obtained [12] as follows:

$$\mu_x = \sum_{ij} \mu_x^{ij}\, p^{ij} \tag{3}$$

where p^{ij} is the fractional population of subband i of valley j. Once individual mobility components are known, the apparent total mobility can be calculated according to Matthiessen's rule as follows:

$$\frac{1}{\mu_{{\rm tot},\,M}} = \frac{1}{\mu_{\rm ph}} + \frac{1}{\mu_{\rm sr}} + \frac{1}{\mu_{\rm imp}}. \tag{4}$$

This leads to the error of applying Matthiessen's rule to the total mobility reproduction, i.e.,

$$E_r = \frac{\mu_{{\rm tot},\,M} - \mu_{\rm tot}}{\mu_{\rm tot}}. \tag{5}$$

III. Semi-Empirical Model

To illustrate the establishment of a semi-empirical model for the error E_r of Matthiessen's rule, we took Takagi *et al.*'s bulk data [4] of electron inversion-layer mobility, as plotted in Fig. 1 versus the effective electric field $E_{\rm eff}$. Here, $E_{\rm eff} = q(0.5N_{\rm inv} + N_{\rm dep})/\varepsilon_s$, where $N_{\rm inv}$ is the inversion-layer density, $N_{\rm dep}$ is the substrate depletion density, and ε_s is the silicon permittivity. Through the aforementioned mobility simulation, a fairly good reproduction of the data, i.e., both the substrate doping concentration dependence and the temperature dependence, was achieved over $E_{\rm eff}$. The corresponding material and/or physical parameters as labeled in the figure are all reasonable compared with those of Takagi *et al.* [14]. This experimentally validates the mobility simulation work here.

Fig. 1 clearly shows the presence of a universal mobility curve. Particularly, the larger the substrate doping concentration $N_{\rm sub}$, the narrower the range of $E_{\rm eff}$ dominated by both phonon scattering and surface roughness scattering. Corresponding calculated values of phonon-limited mobility $\mu_{\rm ph}$, surface-roughness-limited mobility $\mu_{\rm sr}$, and impurity-Coulomb-limited mobility $\mu_{\rm imp}$, are shown in Fig. 2 for $N_{\rm sub} = 10^{17}$ cm^{-3}. Straightforwardly, the apparent total mobility and, hence, error E_r, can be obtained. Remarkably, we found that the largest error $E_{r,\,\max}$ occurs at critical $E_{\rm eff}$, where $\mu_{\rm ph}$ is nearly equal to $\mu_{\rm sr}$, and apart from this point, the errors decrease gradually, as shown in Fig. 2. Specifically, this criterion lies in the high-$E_{\rm eff}$ region ($>$ 1 MV/cm) where impurity Coulomb scattering is weak. This indicates that the relative strength [1] responsible for the errors stem primarily from two distinct components: $\mu_{\rm ph}$ and $\mu_{\rm sr}$. The other origin [3], namely the fractional population

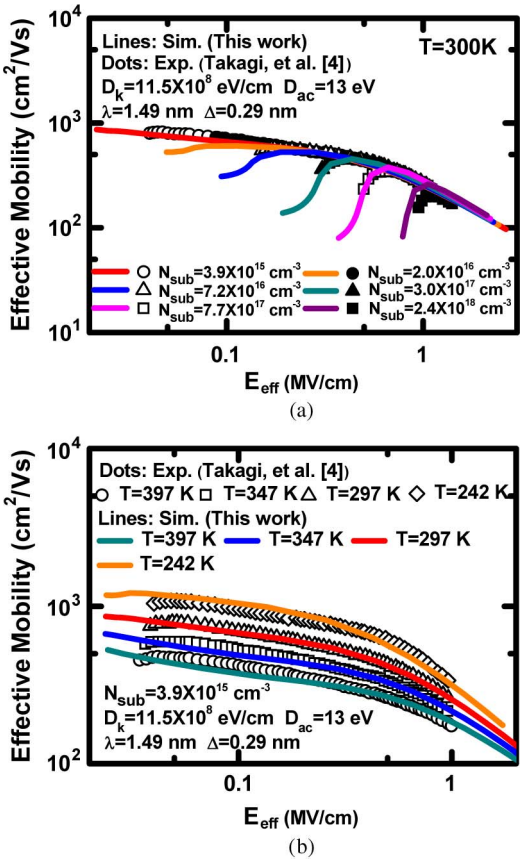

Fig. 1. (Symbols) Electron effective mobility data [4] for (a) six substrate doping concentrations at 300 K and (b) four temperatures for a fixed substrate doping concentration plotted versus vertical effective electric field $E_{\rm eff}$. (Lines) Simulated total mobility curves are shown. $D_{\rm ac}$ is the acoustic deformation potential, D_k is the deformation potential of the kth intervalley phonon, λ is the surface roughness correlation length, and Δ is the surface roughness RMS height.

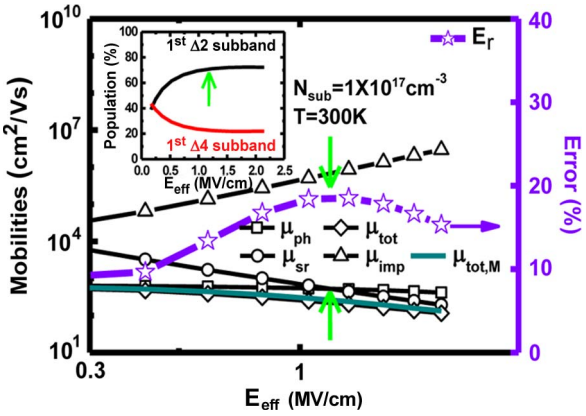

Fig. 2. Simulated total mobility, phonon-limited mobility, surface-roughness-limited mobility, and ionized-impurity-limited mobility versus $E_{\rm eff}$ for $N_{\rm sub} = 10^{17}$ cm^{-3} at 300 K. The apparent total mobility obtained by Matthiessen's rule and, hence, the errors, are together plotted. The arrow indicates the critical $E_{\rm eff}$, where phonon-limited mobility and surface-roughness-limited mobility have the same value. The inset shows the corresponding population of two lowest subbands.

p_o [i.e., p^{11} in (3)] of the twofold lowest subband, can be drawn under $\mu_{\rm ph} = \mu_{\rm sr}$, as shown in the inset of the figure. We also found that an increase in temperature and a decrease in $N_{\rm sub}$ can both increase $E_{r,\,\max}$. In Fig. 3, we show a scatter plot

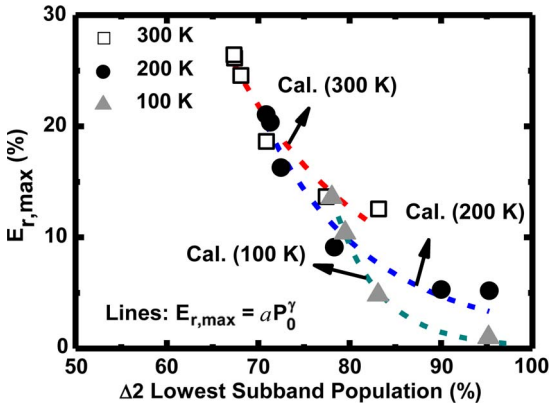

Fig. 3. (Symbols) Scatter plot of the simulated peak error and the corresponding lowest subband population, created from different substrate doping concentrations (10^{14} to 10^{18} cm^{-3}), with temperature as a parameter. (Lines) The calculated results using (6) are shown.

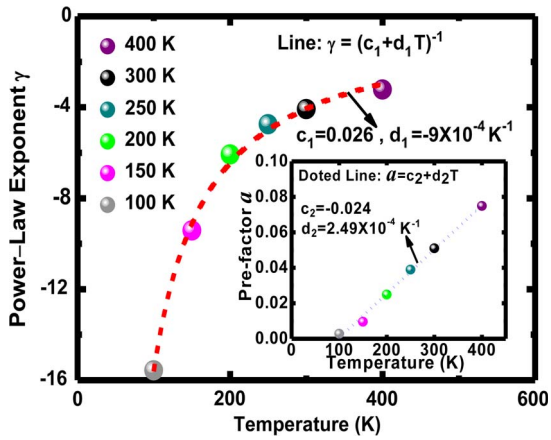

Fig. 4. (Symbols) Extracted power-law exponent γ in (6) versus temperature. (Line) The best fitting is shown. The inset depicts the case of the prefactor a.

between peak error $E_{r,\max}$ and the corresponding p_o for all substrate doping concentrations (10^{14} to 10^{18} cm^{-3}), with the temperature as a parameter. Clearly, a power-law relationship exists between the two, i.e.,

$$E_{r,\max} = ap_o^{\gamma} \tag{6}$$

where a is the prefactor, and γ is the power-law exponent. Different temperatures correspond to different values of a and γ, as depicted in Fig. 4. Two fitting lines can be drawn therein, yielding $a = -0.024 + 2.49 \times 10^{-4}$ T and $\gamma = 1/(0.026 - 9 \times 10^{-4}\,\mathrm{T})$, regardless of doping concentrations.

Then, taking into account the relative strength of $\mu_{\rm ph}$ and $\mu_{\rm sr}$, a semi-empirical model results

$$E_r = E_{r,\max}\left(1 - \alpha \exp\left(\beta \frac{\min(\mu_{\rm ph}, \mu_{\rm sr})}{\max(\mu_{\rm ph}, \mu_{\rm sr})}\right)\right). \tag{7}$$

Equation (7) was obtained by the observation of the distribution of E_r around the critical point. As shown in Fig. 2, the decreasing rate of E_r is faster for $\mu_{\rm ph} < \mu_{\rm sr}$ than $\mu_{\rm ph} > \mu_{\rm sr}$. This is reflected in prefactor α. The falling trend can be treated with an exponent of β times $\mu_{\rm ph}/\mu_{\rm sr}$ or $\mu_{\rm sr}/\mu_{\rm ph}$. Through a best fitting, we obtained $\beta = -5$, and $\alpha = 1$ and 2 for $\mu_{\rm ph} < \mu_{\rm sr}$ and $\mu_{\rm ph} > \mu_{\rm sr}$, respectively. The errors calculated using (6) and

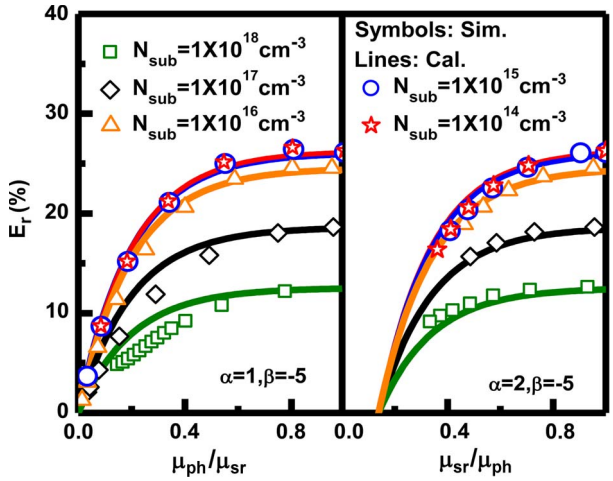

Fig. 5. Comparison of (symbols) simulated and (lines) calculated errors for five different substrate doping concentrations at 300 K, plotted as a function of the ratio of phonon-limited mobility and surface-roughness-limited mobility.

(7) were all confirmed by simulation, as shown in Fig. 5, for a temperature of 300 K. Note that under the critical situation of $\mu_{\rm ph} = \mu_{\rm sr}$, E_r in (7) reduces to its peak value $E_{r,\max}$.

IV. Error-Free Method and Discussion

Combining (4) and (5), we reach the goal in terms of the error-free version of Matthiessen's rule as follows:

$$\frac{1}{\mu_{\rm tot}} = \left(\frac{1}{\mu_{\rm ph}} + \frac{1}{\mu_{\rm sr}} + \frac{1}{\mu_{\rm imp}}\right)(1 + E_r). \tag{8}$$

As justified above, only in the universal mobility region can the effect of impurity Coulomb scattering on E_r be neglected. This means that E_r in (8) can be obtained using (6) and (7), for the case that $\mu_{\rm ph}$, $\mu_{\rm sr}$, and $\mu_{\rm imp}$ are known. In doing so, only the self-consistent solving of coupled Poisson and Schrödinger's equations is needed, with an aim to determine the critical $E_{\rm eff}$ under $\mu_{\rm ph} = \mu_{\rm sr}$ and, hence, p_o. Once p_o is known, maximum error $E_{r,\max}$ and error E_r both can be readily determined. This leads to the actual inversion-layer mobility in the universal mobility region according to (8).

Reciprocally speaking, the method can hold in the assessment of $\mu_{\rm ph}$ and $\mu_{\rm sr}$, given the universal mobility data [4]. To facilitate the process, we assume that $\mu_{\rm ph}$ is independent of $E_{\rm eff}$ and $\mu_{\rm sr}$ follows a power-law dependence on $E_{\rm eff}$. In this situation, error E_r was calculated accordingly while at the same time solving (8). This process is iterated. The result is shown in Fig. 6. In addition, shown in the figure is the case of the conventional use of Matthiessen's rule. It can be seen that large discrepancies occur in the conventional extraction.

At this point, we want to stress the general aspects of the error-free proposal. First, to make possible the application of the method in strain case, we used a previously established strain quantum simulator [10]. The same procedure was again executed, resulting in a scatter plot of simulated $E_{r,\max}$ and p_o, as shown in Fig. 7 for a uniaxial tensile stress of 500 MPa. Noticeably, the effect of strain is primarily to increase p_o. In this strain case, the power-law relationship (6) again holds, as depicted in the figure.

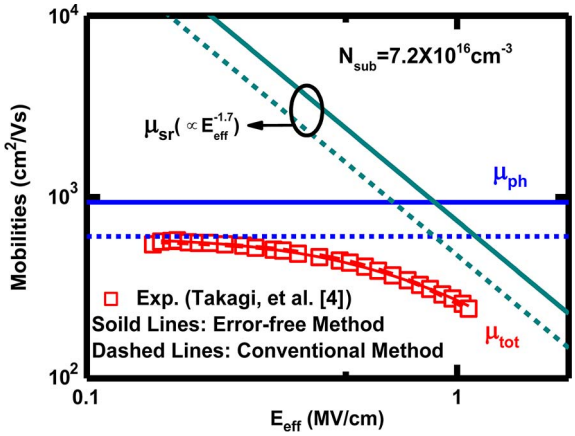

Fig. 6. Phonon-limited mobility and surface-roughness-limited mobility extracted from the universal mobility data [4], using two different methods of applying Matthiessen's rule: (solid lines) the error-free one and (dashed lines) the conventional one.

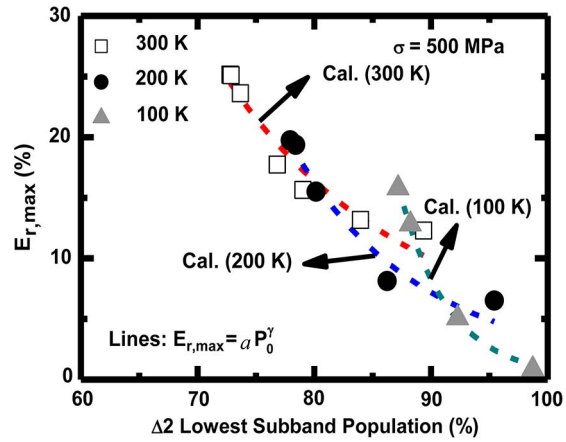

Fig. 7. (Symbols) Scatter plot corresponding to Fig. 3 but under a uniaxial tensile stress of 500 MPa. (Lines) The calculation results came from (6) with $a = -0.018 + 2.69 \times 10^{-4}$ T and $\gamma = 1/(0.042 - 9 \times 10^{-4}$ T).

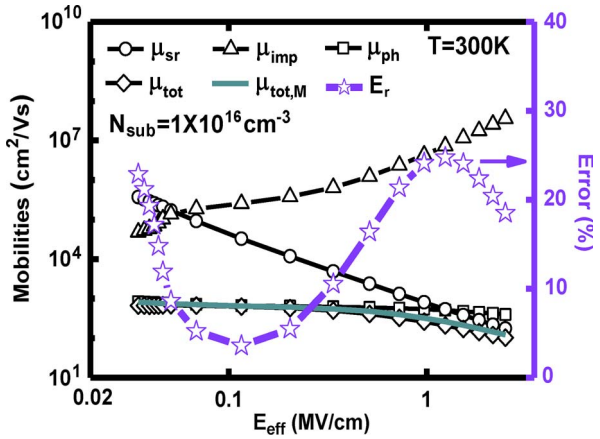

Fig. 8. Simulated total mobility, phonon-limited mobility, surface-roughness-limited mobility, and ionized-impurity-limited mobility versus $E_{\rm eff}$ for $N_{\rm sub} = 10^{16}$ cm^{-3} at 300 K. The apparent total mobility obtained by Matthiessen's rule and the corresponding errors are together plotted.

Second, to examine the errors of Matthiessen's rule in the impurity Coulomb scattering dominant region, we show in Fig. 8 the simulated mobility components for $N_{\rm sub} = 10^{16}$ cm^{-3} at 300 K, along with those from Matthiessen's rule and the corresponding errors. Obviously, in the low-$E_{\rm eff}$ region ($<$ 0.1 MV/cm), the error increases with decreasing $E_{\rm eff}$. The corresponding errors at 300 K are plotted in Fig. 9 versus the ratio of $\mu_{\rm ph}$ to $\mu_{\rm imp}$, with the substrate doping concentration as a parameter. We found that the same coefficients can work: $\beta = -5$ and $\alpha = 1$. The corresponding semi-empirical model is

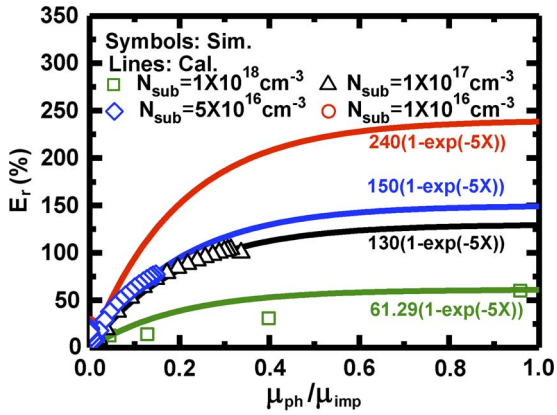

Fig. 9. Comparison of (symbols) simulated and (lines) calculated errors for four different substrate doping concentrations at 300 K, plotted as a function of the ratio of phonon-limited mobility to impurity-Coulomb-limited mobility.

$$E_r = E_{r,\max}\left(1 - \exp(-5\mu_{\rm ph}/\mu_{\rm imp})\right) \tag{9}$$

with $E_{r,\max} = 3 \times 10^6$ N$_{\rm sub}^{-0.26}$. The fitting is good, thus verifying the applicability of the proposed model. Further, Fig. 10 shows the simulated impurity-Coulomb-limited mobility $\mu_{\rm imp}$, the apparent impurity-Coulomb-limited mobility $\mu_{{\rm imp},M}$ from the conventional use of Matthiessen's rule, and the error of extracting $\mu_{{\rm imp},M}$ (see [6] for the definition of the extraction error). Reasonable agreements with those of Esseni and Driussi [6] are evident, again supporting the simulation work here. Indeed, devising another model for the extraction error is challenging and needs to be investigated further. In this sense, our proposed model in this paper may be helpful because, according to the work by Esseni and Driussi [6], a certain relationship exists between the global error [i.e., E_r in (5)] and the local error (i.e., the extraction error of the individual mobility component).

Third, in the case of high-k/metal-gate (HKMG) bulk MOSFETs, it can be intuitively drawn that *in the universal mobility region*, the proposed semi-empirical error model can work, provided that remote scattering is insignificant as in the case of the impurity Coulomb scattering aforementioned. If that is not the fact, however, a sophisticated numerical simulation task is needed to reproduce HKMG mobility data, with remote scattering mechanisms taken into account. In this sense, (1) is augmented to be

$$\frac{1}{\tau_{\rm tot}^{ij}(E)} = \frac{1}{\tau_{\rm ph}^{ij}(E)} + \frac{1}{\tau_{\rm sr}^{ij}(E)} + \frac{1}{\tau_{\rm imp}^{ij}(E)} + \frac{1}{\tau_{\rm add}^{ij}(E)} \tag{10}$$

where $\tau_{\rm add}$ is the relaxation time due to additional scattering alone. One of the $\tau_{\rm add}$ expressions due to optical phonons

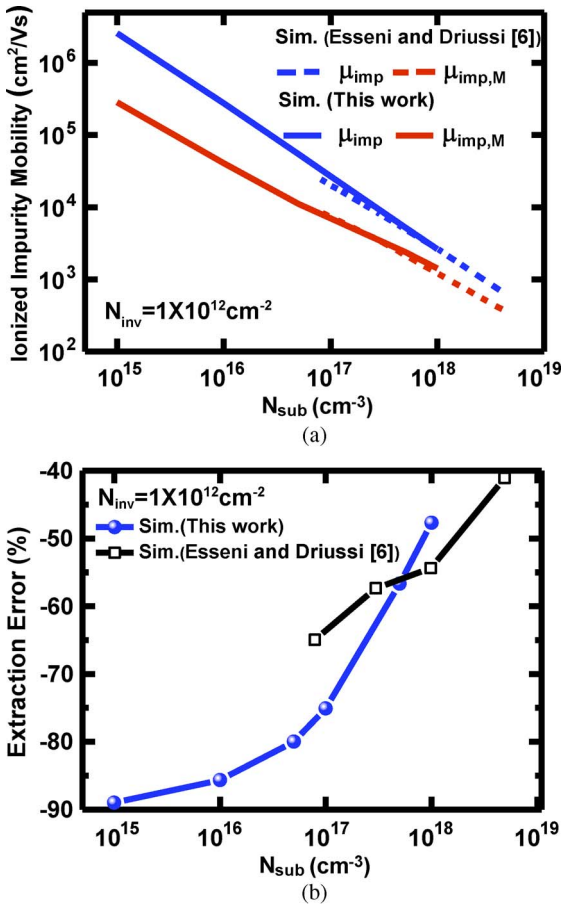

Fig. 10. Comparison of (a) simulated and extracted impurity-Coulomb-limited mobility and (b) corresponding errors in this paper with those of [6], plotted as a function of substrate doping concentration.

in high-k dielectric can be found elsewhere [18]. The corresponding error-free Matthiessen's rule may be devised in a similar way.

Finally, we want to state that the presented semi-empirical error model should be, in principle, applicable to the double-gate case or the FinFET case. Particularly, the model predicts an increase in the error of Matthiessen's rule if the doping concentration of the film is decreased. However, as the film thickness decreases, the mobility expressions used in this paper fail and deteriorate the quality of the model. To overcome this, one has to turn to the literature sources [13], [19]–[21] concerning the mobility expressions suitable for thin-film structures and extra scatterers. Then, the corresponding error-free Matthiessen's rule should be able to be produced in the context of the key origins of the errors [1], [3].

V. Conclusion

Through the experimentally validated electron inversion-layer mobility simulation, a semi-empirical model for the errors of Matthiessen's rule has been established for a single-gate bulk MOSFET in the universal mobility region. The error-free version of Matthiessen's rule has straightforwardly been obtained. To make the error-free proposal more general, we have elaborated on several challenging issues.

References

[1] F. Stern, "Calculated temperature dependence of mobility in silicon inversion layers," *Phys. Rev. Lett.*, vol. 44, no. 22, pp. 1469–1472, Jun. 1980.

[2] J. Li and T. P. Ma, "Scattering of silicon inversion layer electrons by metal/oxide interface roughness," *J. Appl. Phys.*, vol. 62, no. 10, pp. 4212–4215, Nov. 1987.

[3] M. V. Fischetti, F. Gámiz, and W. Hänsch, "On the enhanced electron mobility in strained-silicon inversion layers," *J. Appl. Phys.*, vol. 92, no. 12, pp. 7320–7324, Dec. 2002.

[4] S. Takagi, A. Toriumi, M. Iwase, and H. Tango, "On the universality of inversion layer mobility in Si MOSFETs: Part I—Effects of substrate impurity concentration," *IEEE Trans. Electron Devices*, vol. 41, no. 12, pp. 2357–2362, Dec. 1994.

[5] J. R. Hauser, "Extraction of experimental mobility data for MOS devices," *IEEE Trans. Electron Devices*, vol. 43, no. 11, pp. 1981–1988, Nov. 1996.

[6] D. Esseni and F. Driussi, "A quantitative error analysis of the mobility extraction according to the Matthiessen rule in advanced MOS transistors," *IEEE Trans. Electron Devices*, vol. 58, no. 8, pp. 2415–2422, Aug. 2011.

[7] M. J. Chen, S. C. Chang, S. J. Kuang, C. C. Lee, W. H. Lee, K. H. Cheng, and Y. H. Zhan, "Temperature-dependent remote-Coulomb-limited electron mobility in n^+-polysilicon ultrathin gate oxide nMOSFETs," *IEEE Trans. Electron Devices*, vol. 58, no. 4, pp. 1038–1044, Apr. 2011.

[8] M. J. Chen, C. C. Lee, and K. H. Cheng, "Hole effective masses as a booster of self-consistent six-band k · p simulation in inversion layers of pMOSFETs," *IEEE Trans. Electron Devices*, vol. 58, no. 4, pp. 931–937, Apr. 2011.

[9] M. J. Chen, L. M. Chang, S. J. Kuang, C. W. Lee, S. H. Hsieh, C. A. Wang, S. C. Chang, and C. C. Lee, "Temperature-oriented mobility measurement and simulation to assess surface roughness in ultrathin-gate-oxide ($\sim$1 nm) nMOSFETs and its TEM evidence," *IEEE Trans. Electron Devices*, vol. 59, no. 4, pp. 949–955, Apr. 2012.

[10] M. J. Chen and W. H. Lee, "Evidence for the fourfold-valley confinement electron piezo-effective-mass coefficient in inversion layers of ⟨110⟩ uniaxial-tensile-strained (001) nMOSFETs," *IEEE Electron Device Lett.*, vol. 33, no. 6, pp. 755–757, Jun. 2012.

[11] F. Stern, "Self-consistent results for n-type Si inversion layers," *Phys. Rev. B, Condens. Matter*, vol. 5, no. 12, pp. 4891–4899, Jun. 1972.

[12] D. K. Ferry and S. M. Goodnick, *Transport in Nanostructures*. Cambridge, U.K.: Cambridge Univ. Press, 1999.

[13] D. Esseni, P. Palestri, and L. Selmi, *Nanoscale MOS Transistors: Semi-Classical Transport and Applications*. Cambridge, U.K.: Cambridge Univ. Press, 2011.

[14] S. Takagi, J. L. Hoyt, J. J. Welser, and J. F. Gibbons, "Comparative study of phonon-limited mobility of two-dimensional electrons in strained and unstrained Si metal–oxide–semiconductor field-effect transistors," *J. Appl. Phys.*, vol. 80, no. 3, pp. 1567–1577, Aug. 1996.

[15] Yamakawa, H. Ueno, K. Taniguchi, C. Hamaguchi, K. Miyatsuji, K. Masaki, and U. Ravaioli, "Study of interface roughness dependence of electron mobility in Si inversion layers using the Monte Carlo method," *J. Appl. Phys.*, vol. 79, no. 2, pp. 911–916, Jan. 1996.

[16] M. Lundstrom, *Fundamentals of Carrier Transport*, 2nd ed. Cambridge, U.K.: Cambridge Univ. Press, 2009.

[17] K. Hirakawa and H. Sakaki, "Mobility of the two-dimensional electron gas at selectively doped n -type $Al_xGa_{1-x}As$/GaAs heterojunctions with controlled electron concentrations," *Phys. Rev. B, Condens. Matter*, vol. 33, no. 12, pp. 8291–8303, Jun. 1986.

[18] M. V. Fischetti, T. P. O'Regan, S. Narayanan, C. Sachs, S. Jin, J. Kim, and Y. Zhang, "Theoretical study of some physical aspects of electronic transport in nMOSFETs at the 10-nm gate-length," *IEEE Trans. Electron Devices*, vol. 54, no. 9, pp. 2116–2136, Sep. 2007.

[19] F. Gámiz, J. A. Lüpez-Villanueva, J. B. Roldán, J. E. Carceller, and P. Cartujo, "Monte Carlo simulation of electron transport properties in extremely thin SOI MOSFETs," *IEEE Trans. Electron Devices*, vol. 45, no. 5, pp. 1122–1126, May 1998.

[20] D. Esseni, A. Abramo, L. Selmi, and E. Sangiorgi, "Physically based modeling of low field electron mobility in ultrathin single- and double-gate SOI n-MOSFETs," *IEEE Trans. Electron Devices*, vol. 50, no. 12, pp. 2445–2455, Dec. 2003.

[21] D. Esseni, "On the modeling of surface roughness limited mobility in SOI MOSFETs and its correlation to the transistor effective field," *IEEE Trans. Electron Devices*, vol. 51, no. 3, pp. 394–401, Mar. 2004.

Ming-Jer Chen (S'78–M'79–SM'98) has been with the Department of Electronics Engineering, NCTU, since 1985, and is currently a Full Professor.

Wei-Han Lee (S'09) received the B.S. degree in electrophysics and the Ph.D. degree in electronics engineering from National Chiao Tung University, Hsinchu, Taiwan, in 2005 and 2012, respectively.

Yi-Hui Huang received the B.S. degree in applied science from National Hsinchu University of Education, Hsinchu, Taiwan, in 2010 and the M.S. degree in electronics engineering from National Chiao Tung University, Hsinchu, in 2012.